Available online at www.sciencedirect.com

SciVerse ScienceDirect

Ceramics International 38 (2012) 2201–2207

CERAMICS INTERNATIONAL

www.elsevier.com/locate/ceramint

Carbothermal production of ZrB_2–ZrO_2 ceramic powders from ZrO_2–B_2O_3/B system by high-energy ball milling and annealing assisted process

Özge Balcı*, Duygu Ağaoğulları, İsmail Duman, M. Lütfi Öveçoğlu

İstanbul Technical University, Faculty of Chemical and Metallurgical Engineering, Department of Metallurgical and Materials Engineering, Ayazağa Campus, 34469 Maslak, Istanbul, Turkey

Received 7 October 2011; received in revised form 24 October 2011; accepted 25 October 2011
Available online 29 October 2011

Abstract

Zirconium diboride (ZrB_2)-zirconium dioxide (ZrO_2) ceramic powders were prepared by comparing two different boron sources as boron oxide (B_2O_3) and elemental boron (B). The production method was high-energy ball milling and subsequent annealing of powder blends containing stoichiometric amounts of ZrO_2, B_2O_3/B powders in the presence of graphite as a reductant. The effects of milling duration (0, 2 and 6 h), annealing duration (6 and 12 h) and annealing temperature (1200–1400 °C) on the formation and microstructure of ceramic powders were investigated. Phase, thermal and microstructural characterizations of the milled and annealed powders were performed by X-ray diffractometer (XRD), differential scanning calorimeter (DSC) and transmission electron microscope (TEM). The formation of ZrB_2 starts after milling for 2 h and annealing at 1300 °C if B_2O_3 is used as boron source and after milling for 2 h and annealing at 1200 °C if B is used as boron source.

Keywords: A. Milling; D. Borides; D. Carbon; D. ZrO_2; Annealing

1. Introduction

ZrB_2-based ceramics have been broadly investigated in recent years due to their outstanding properties such as high melting point, high electrical and thermal conductivity and high chemical inertness [1,2]. These properties make them significant for high temperature applications and they are commonly referred to as ultra-high temperature ceramics (UHTCs) [3]. ZrB_2 ceramics attract considerable interest especially in the areas where corrosion-wear-oxidation resistance is demanded [2,4] such as high-temperature electrodes, molten metal crucibles, thermal protection systems for hypersonic flight, atmospheric re-entry vehicles and nose caps [5–7].

ZrB_2-based ceramics were fabricated by spark plasma sintering (SPS), hot pressing (HP) and pressureless sintering (PS) with the starting powders of ZrB_2 and required additives such as SiC, ZrC, ZrO_2, $MoSi_2$, AlN, B_4C, Al_2O_3, etc. [8–15]. Preparation of ZrB_2–ZrO_2 ceramics with these methods have been also reported using ZrB_2 and ZrO_2 as starting materials [2,16–19]. On the other hand, milling processes were only performed for synthesizing ZrB_2 or ZrO_2 powders and also ZrB_2/ZrC powders [20–22]. In addition, zirconium-based ceramics in fine powder form (ZrB_2–SiC–ZrC, ZrB_2–SiC–ZrC–ZrSi) were fabricated via combustion synthesis (CS) [23]. Production of ZrB_2–ZrO_2 ceramic powders by mechanically activated annealing processes is not a well-discussed topic.

In the present study, ZrB_2–ZrO_2 ceramic powders were produced via high-energy ball milling and subsequent annealing of powder blends containing stoichiometric amounts of ZrO_2, B_2O_3/B powders in the presence of graphite as a reductant. The original aspects of this study are production technique and the utilization and comparison of economical raw materials for preparing ZrB_2-based ceramic powders. The results of this study can make new contributions to the current literature as precursors for the development of ZrB_2-based dense bodies.

2. Experimental procedure

Raw materials used in this investigation were zirconium dioxide (ZrO_2, ABCR™, 99% purity, 4.8 μm average particle size), boron oxide (B_2O_3, ETI™ Mine, 98% purity, 466.9 μm

* Corresponding author. Tel.: +90 212 285 6237; fax: +90 212 285 3427.
E-mail addresses: ozgebalci1@yahoo.com (Ö. Balcı), bozkurtdu@itu.edu.tr (D. Ağaoğulları), iduman@itu.edu.tr (İ. Duman), ovecoglu@itu.edu.tr (M.L. Öveçoğlu).

0272-8842/$36.00
doi:10.1016/j.ceramint.2011.10.067

average particle size) and boron (B, ABCR™, 95–97% purity, 50 μm average particle size) powders. Graphite powder (C, Alfa Aesar™, 99% purity, 45 μm average particle size) was used as a reducing agent. The powder blends containing stoichiometric amounts of the raw materials were prepared in accordance with the reactions given in Eqs. (1) and (2). Boron oxide in powder blend 1 (#1) and elemental boron in powder blend 2 (#2) were used as two different boron sources.

$$ZrO_2 + B_2O_3 + 5C = ZrB_2 + 5CO \quad (1)$$

$$ZrO_2 + 2B + 2C = ZrB_2 + 2CO \quad (2)$$

Milling was performed in a Spex™ 8000 D Mixer/Mill with a rotation speed of 1200 rpm using hardened steel balls (6 mm diameter) in a hardened steel vial (50 ml capacity). Powder blends (6 g) were loaded into the milling vial with a ball-to-powder weight ratio (BPR) of 10:1. Before milling, the vials were evacuated to about 10^{-2} Pa and back-filled with Ar gas (BOS™, 99.999% purity) in a Plaslabs™ glove-box. All powder blends were milled for 2 and 6 h. After milling, samples were placed in alumina boats and annealed in a Protherm™ tube furnace under flowing Ar atmosphere (2000 ml/min). Annealing temperatures were 1200, 1300 and 1400 °C with a heating and cooling rate of 10 °C/min. Annealing was conducted with durations of 6 and 12 h.

Microstructural and morphological characterizations of the milled and annealed powders were carried out using a Bruker™ D8 Advanced Series X-Ray Diffractometer (XRD, CuKα radiation in the 2θ range of 20–80°) and a Jeol™ JEM-2000EX Transmission Electron Microscope (TEM, 160 kV). The International Center for Diffraction Data (ICDD) powder diffraction files were utilized in the identification of crystalline phases. The average crystallite size and lattice strain of the milled powders were determined using a Bruker™-AXS TOPAS V3.0 software [24]. Thermal analysis of the products was performed by a TA™ Instruments Q600 Differential Scanning Calorimeter (DSC, in an alumina crucible up to 1400 °C by 10 °C/min under Ar atmosphere). Standard Gibbs free energy and enthalpy changes-temperature relations of the reactions were interpreted by the FactSage™ 6.2 thermo-chemical software.

3. Results and discussion

Fig. 1 shows the standard Gibbs free energy change (ΔG°)-temperature relations of the reactions given in Eqs. (1) and (2). ΔG° of the reactions in Eq. (1) and (2) respectively show negative values starting from 1600 and 1400 °C. Thus, the reaction in Eq. (2) is thermodynamically more feasible than the reaction in Eq. (1) at the same conditions.

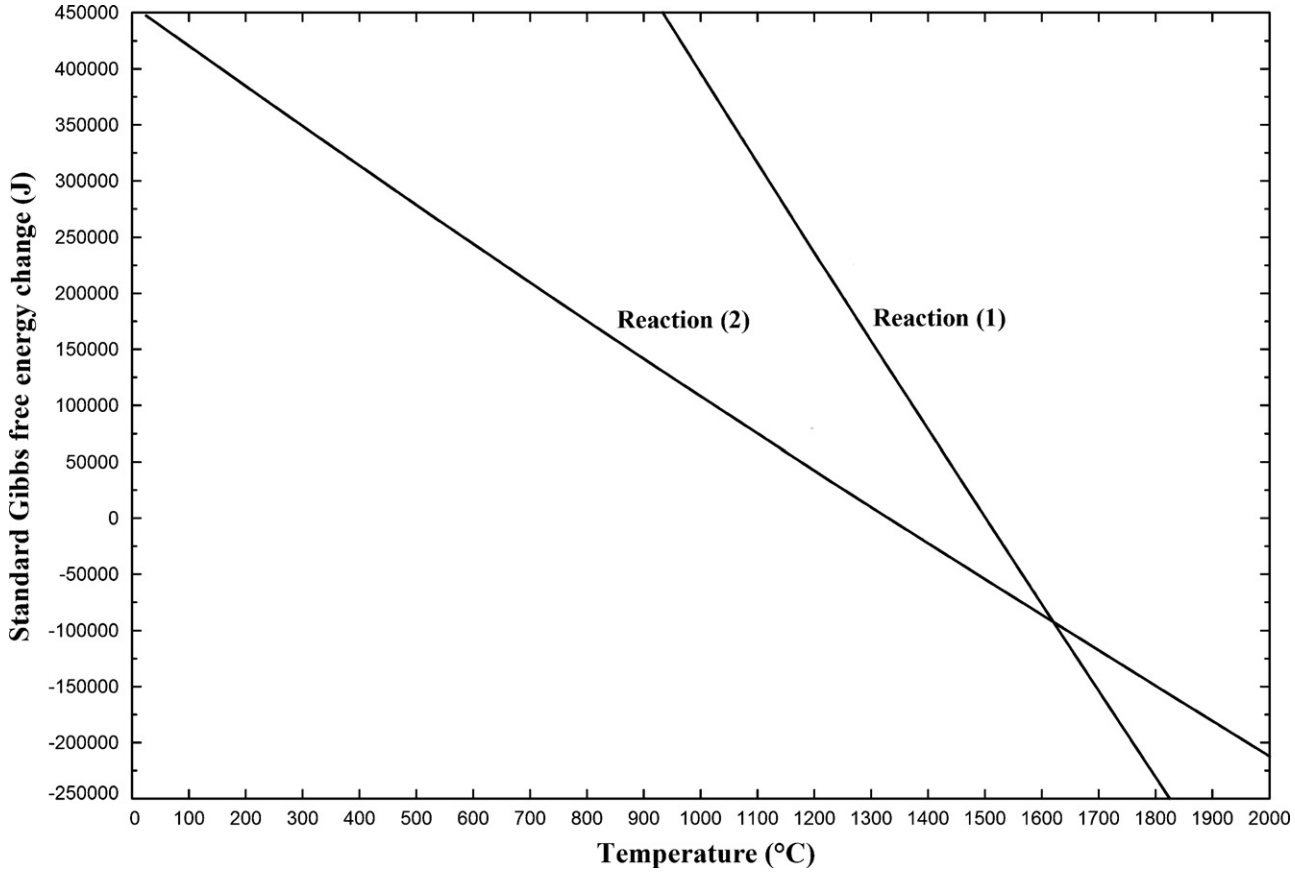

Fig. 1. Standard Gibbs free energy change–temperature relations of the reactions given in Eqs. (1) and (2).

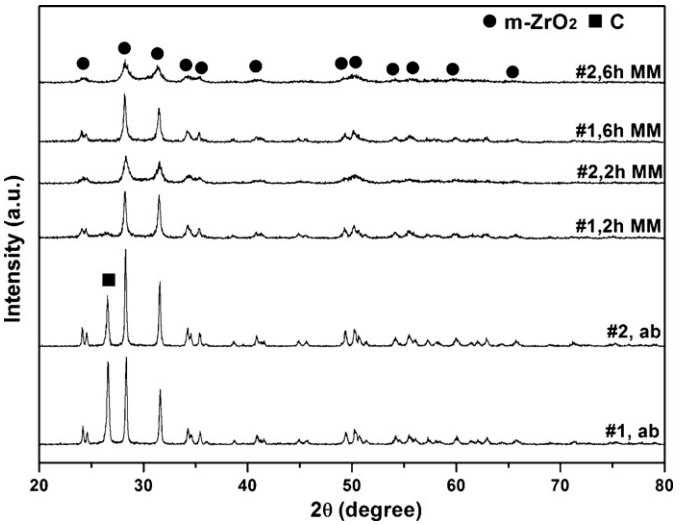

Fig. 2. XRD patterns of as-blended and milled powder blends for different milling durations.

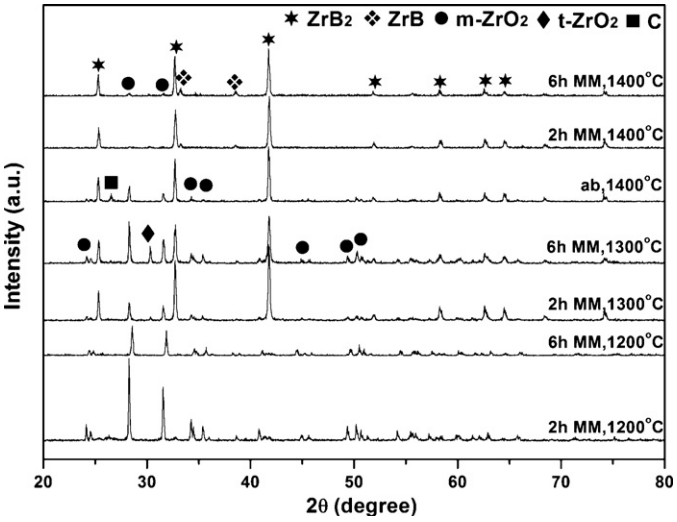

Fig. 3. XRD patterns of #1 milled for different durations and annealed for 12 h at different temperatures.

Fig. 2 illustrates the XRD patterns of the as-blended (ab) and mechanically milled (MM) powder blends for different milling durations. ZrO_2 (ICDD Card No: 74-1200, Bravais lattice: monoclinic, $a = 5.120$ Å, $b = 5.216$ Å, $c = 5.281$ Å) phase with C (ICDD Card No: 26-1080, Bravais lattice: hexagonal, $a = b = 2.456$ Å, $c = 13.392$ Å) is present in the as-blended powders. The absence of boron peaks is believed to be due to its amorphous nature. After milling, C phase completely disappears because of the continuous amorphization during milling. The peaks of ZrO_2 broaden as milling duration increases from 2 to 6 h indicating the decrease in the crystallite size of ZrO_2 with milling. The reason for the difference between the peak intensities of #1 and #2 is high hardness of B (45 GPa) in comparison with the hardness of B_2O_3 (1.5 GPa) which triggers the fracture mechanism [25,26]. Table 1 represents the average crystallite sizes and lattice strains of ZrO_2 particles in the milled powder blends. The average crystallite size of ZrO_2 decreases from 116.5 nm (in the as-blended powder) to 41.5 nm (in the powders MM for 6 h) for #1 and to 10.9 nm (in the powders MM for 6 h) for #2. On the other hand, lattice strain increases up to 0.8255 for #1 and up to 3.2680 for #2. It shows that continuous deformation of powders results in grain refinement and smaller grains in #2.

Table 1
The average crystallite sizes and lattice strains of powder blends and those milled for different durations.

Powder blends	Milling duration	Crystallite size (nm)	Lattice strain (%)
#1	0	116.5	0.2945
	2	43.2	0.7985
	6	41.5	0.8255
#2	0	116.5	0.2945
	2	15.8	2.2250
	6	10.9	3.2680

Fig. 3 shows the XRD patterns of #1 milled at different durations and annealed at different temperatures for 12 h. No reactions take place after annealing at 1200 °C in the powders MM for 2 and 6 h. ZrB_2 (ICDD Card No: 34-0423, Bravais lattice: hexagonal, $a = b = 3.168$ Å, $c = 4.647$ Å) phase emerges in the microstructure after annealing at 1300 °C. Furthermore, t-ZrO_2 (ICDD Card No: 72-7115, Bravais lattice: tetragonal, $a = b = 3.598$ Å, $c = 5.185$ Å) phase is observed with m-ZrO_2 (Bravais lattice: monoclinic). Small amounts of ZrO_2 was transformed from monoclinic to tetragonal structure due to the reduction mechanism of B_2O_3 with C. Annealing at 1400 °C enables the formation of the ZrB_2 phase without ZrO_2, as ZrB (ICDD Card No: 65-8703, Bravais lattice: cubic, $a = b = c = 4.647$ Å) phase occurs in the structure. C phase remains in the as-blended powder annealed at 1400 °C. Thus, after annealing, milled powders

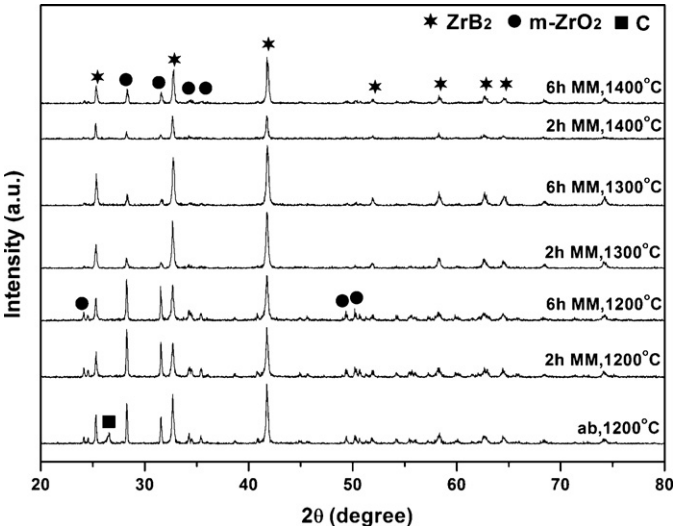

Fig. 4. XRD patterns of #2 milled for different durations and annealed for 12 h at different temperatures.

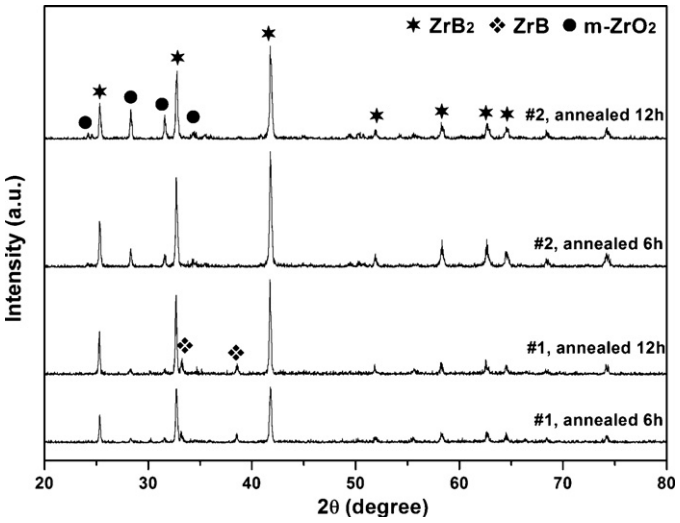

Fig. 5. XRD patterns of 6 h milled powder blends annealed at 1400 °C for different durations.

have higher conversion yields than those of the as-blended powders. These results show that compositional changes during heating occur at a lower temperature of 1300 °C than the theoretical formation temperature (at 1600 °C, Fig. 1) because of the mechanical activation.

Fig. 4 shows the XRD patterns of #2 that milled for different durations and annealed at different temperatures for 12 h. As seen in Fig. 4, as-blended and annealed powders have ZrB_2 and ZrO_2 phase in the presence of C. All powders milled at different durations and annealed at different temperatures comprise the ZrB_2 and ZrO_2 phase together. The peak intensities of ZrB_2 increase with extended milling durations. On the other hand, the peak intensities of ZrB_2 decrease as annealing temperature increases from 1300 to 1400 °C, indicating that the reaction expressed in Eq. (2) is reversed above 1300 °C and hence the peak intensities of ZrO_2 increase. Therefore, the optimum annealing temperature is found as 1300 °C for #2 in order to obtain the ZrB_2-based ceramic powders. These results also show that due to the mechanical activation, phase changes during annealing occur at a lower temperature (at 1200 °C) than the theoretical formation temperature (at 1400 °C). Eventually, XRD patterns prove the formation of ZrB_2–ZrO_2 ceramic powders.

Fig. 5 is the XRD patterns of 6 h milled powder blends annealed at 1400 °C for different annealing durations. Fig. 5 indicates the effect of annealing duration (6 and 12 h) with the comparison of #1 and #2. The peak intensities of ZrB_2 increase with extended annealing duration for #1. The peaks of ZrO_2 for #2 broaden as annealing duration increases from 6 to 12 h, indicating the formation of ZrO_2 in large grain sizes. On the basis of the XRD patterns shown in Figs. 2–5, the main reactions (Eqs. (1) and (2)) occur during annealing which result in the formation of the ZrB_2–ZrO_2 phases together without any intermetallic phase. The best result for #1 obtained from milling for 6 h and annealing at 1400 °C whereas the best result for #2 obtained from milling for 6 h and annealing at 1300 °C during 12 h. According to the net area calculation method from XRD patterns, ZrB_2–ZrO_2 ceramic powders were obtained with a content range of ZrO_2 4 vol.% for #1 and 9 vol.% for #2. An example of the usage of ZrB_2–ZrO_2 powders is given in the current literature for the production of Al_2O_3/ZrB_2/ZrO_2 ceramic composites [13,14].

Fig. 6 shows the DSC thermograms of as-blended and milled powders. DSC analyses were carried out up to 1400 °C in order to investigate the compositional changes or phase transformations during heating. DSC thermograms of as-blended powders exhibit only small endothermic peaks. On the other hand, DSC thermograms of 2 h milled powders have a clear and sharp endothermic peak at about 1150 °C, indicating the transformation of ZrO_2 from monoclinic to tetragonal structure [27]. In addition, the endothermic peaks of 2 h milled powders at 1220 °C for #1 and 1190 °C for #2 can be attributed to the formation of the ZrB_2 phase. Thus, the broad endothermic peak at 1320 °C shows the formation of ZrB_2 and ZrB phases together for 6 h milled #1. DSC thermograms of 6 h milled #2 do not give any sharp peaks due to its very small particle sizes. These results are in good agreement with the XRD patterns. Fig 7a and b illustrates the enthalpy change–temperature relations of the reactions given in Eqs. (1) and (2), respectively. The general trend of the enthalpy change according to the temperature is similar with DSC thermograms of as-blended powders (Fig. 6). The declines of enthalpy at 449.85 °C (Fig. 7a) and at 1207.45 °C (Fig. 7a and b) indicate the melting of B_2O_3 and the phase transformation of ZrO_2 from monoclinic to tetragonal, respectively. It supports the interpretations of DSC thermograms (Fig. 6). However, the formation of ZrB_2 was not observed from the FactSage diagrams since they are only for equilibrium conditions. Due to the fact that milling process is far from equilibrium; synthesized phases are not expected to be compatible with all thermodynamically calculated phases. Experimental and theoretical investigations show that mechanical activation triggers the formation of ZrB_2 after annealing at lower temperatures for both kinds of boron sources.

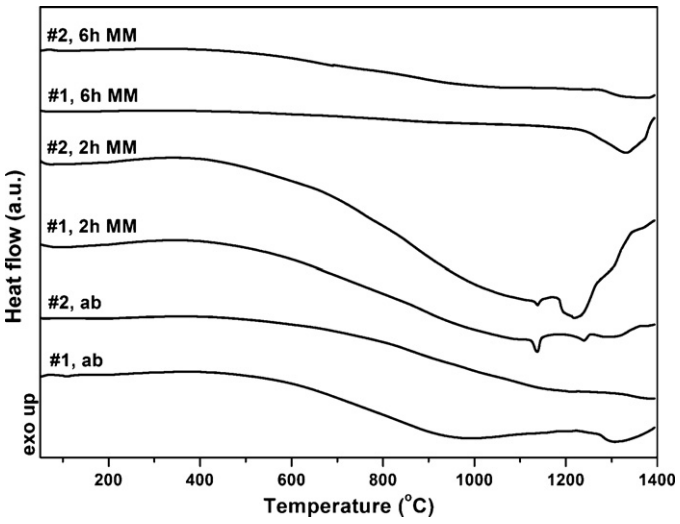

Fig. 6. DSC thermograms of as-blended and milled powder blends.

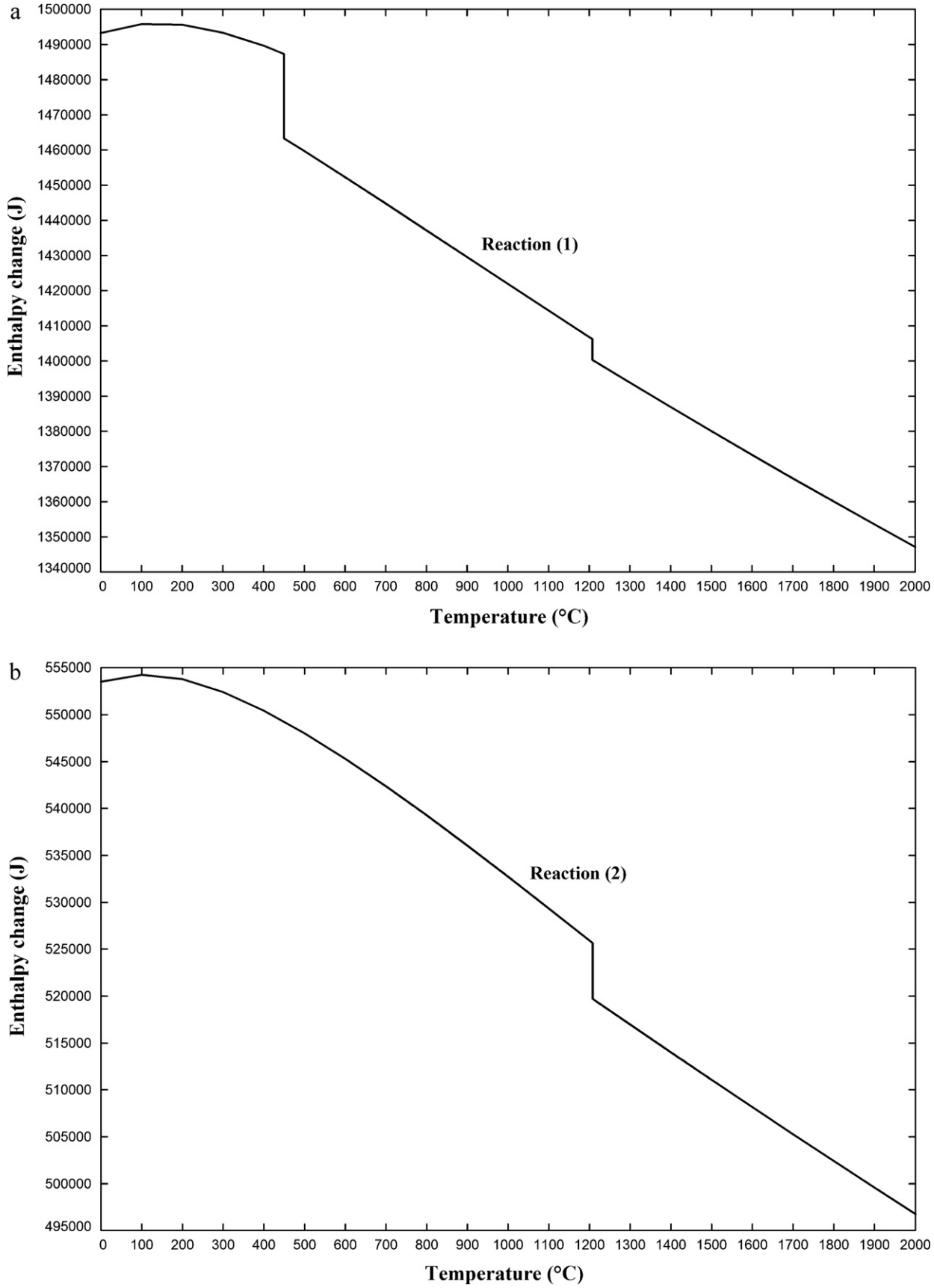

Fig. 7. Enthalpy change–temperature relations of the reactions given in: (a) Eq. (1) and (b) Eq. (2).

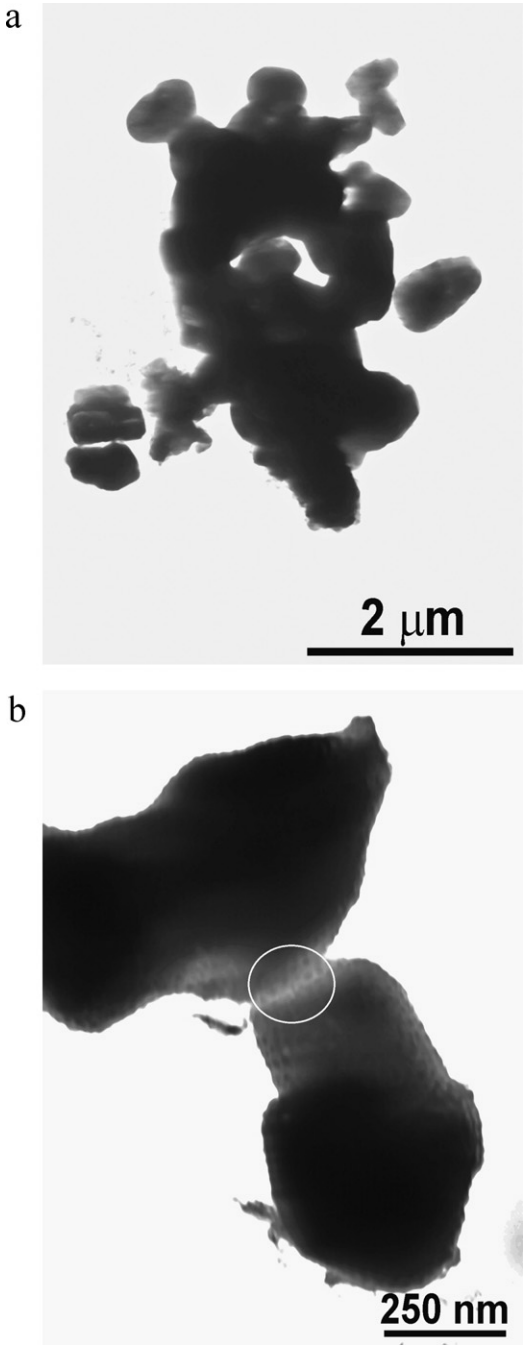

Fig. 8. TEM micrographs of #1 milled for 6 h and annealed at 1400 °C during 12 h: (a), (b) bright-field images.

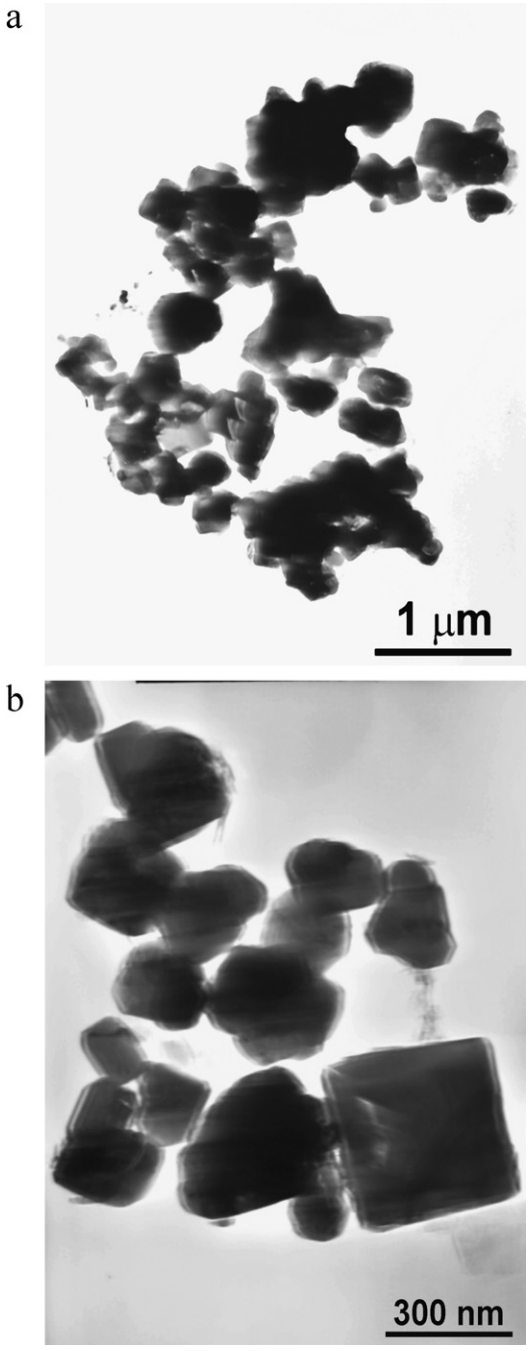

Fig. 9. TEM micrographs of #2 milled for 6 h and annealed at 1300 °C during 12 h: (a), (b) bright-field images.

Fig. 8a and b represents the TEM micrographs (bright field) taken from an agglomerate of #1 milled for 6 h and annealed at 1400 °C during 12 h. It reveals the presence of ZrB_2 and ZrO_2 particles ranging in size between 500 and 800 nm. The powder particles are observed larger than its original sizes because of necking. White circled region in Fig. 8b gives the neck formation arised by high temperature. Fig. 9a and b illustrates the TEM micrographs taken from an agglomerate of #2 milled for 6 h and annealed at 1300 °C during 12 h. It reveals the presence of ZrB_2 and ZrO_2 particles ranging in size between 100 and 300 nm. The use of low temperature and elemental boron as boron source lead the formation of smaller particles after annealing.

4. Conclusions

Milling and subsequent annealing of the powder blends of ZrO_2, B_2O_3/B and C was successfully utilized in the fabrication of ZrB_2–ZrO_2 ceramic powders with fine microstructure as precursors of composites. Fabrication of ZrB_2–ZrO_2 ceramic

powders was achieved in the current study from economical raw materials and at lower temperatures by means of the mechanical activation before annealing. XRD investigations of as-blended and milled powders show that smaller particles were obtained with increasing milling time and the use of B as boron source. The formation of ZrB_2 starts after milling for 2 h and annealing at 1300 °C if B_2O_3 is used as boron source and milling for 2 h and annealing at 1200 °C if B is used as boron source. The best result for the powder blend $ZrO_2/B_2O_3/C$ was obtained from milling for 6 h and annealing at 1400 °C whereas the best result for the powder blend ZrO_2/B/C was obtained from milling for 6 h and annealing at 1300 °C during 12 h. The use of elemental boron as boron source causes the formation of smaller particles than the use of boron oxide, both after milling and annealing.

Acknowledgement

The authors would like to express their appreciations to Aziz Genç for his help in TEM experiments.

References

[1] F. Monteverde, S. Guicciardi, A. Bellosi, Advances in microstructure and mechanical properties of zirconium diboride based ceramics, Mater. Sci. Eng. A 346 (2003) 310–319.
[2] W. Li, X. Zhang, C. Hong, W. Han, J. Han, Preparation, microstructure and mechanical properties of ZrB_2–ZrO_2 ceramics, J. Eur. Ceram. Soc. 29 (2009) 779–786.
[3] W.G. Fahrenholtz, G.E. Hilmas, Refractory diborides of zirconium and hafnium, J. Am. Ceram. Soc. 90 (2007) 1347–1364.
[4] T. Zhu, W. Li, X. Zhang, P. Hu, C. Hong, L. Weng, Oxidation behavior of ZrB_2–SiC–ZrO_2 ceramic composites in the temperature range of 800–1200 °C, Mater. Chem. Phys. 116 (2009) 593–598.
[5] A.L. Chamberlain, W.G. Fahrenholtz, G.E. Hilmas, High-strength zirconium diboride-based ceramics, J. Am. Ceram. Soc. 87 (2004) 1170–1172.
[6] M. Brouchu, B.D. Gauntt, L. Boyer, R.E. Loehman, Pressureless reactive sintering of ZrB_2 ceramics, J. Eur. Ceram. Soc. 29 (2009) 1493–1499.
[7] J.J. Melendez-Martinez, A. Dominguez-Rodriguez, F. Monteverde, C. Melandri, G. Portu, Characterisation and high temperature mechanical properties of zirconium boride-based materials, J. Eur. Ceram. Soc. 22 (2002) 2543–2549.
[8] S. Guo, Densification of ZrB_2-based composites and their mechanical and physical properties: a review, J. Eur. Ceram. Soc. 29 (2009) 995–1011.
[9] F. Monteverde, A. Bellosi, L. Scatteia, Processing and properties of ultra-high temperature ceramics for space applications, Mater. Sci. Eng. A 485 (2008) 415–421.
[10] D. Chen, W. Li, X. Zhang, P. Hu, J. Han, C. Hong, W. Han, Microstructural feature and thermal shock behaviour of hot-pressed ZrB_2–SiC–ZrO_2 composite, Mater. Chem. Phys. 116 (2009) 348–352.
[11] F. Monteverde, A. Bellosi, S. Guicciardi, Processing and properties of zirconium diboride-based composites, J. Eur. Ceram. Soc. 22 (2002) 279–288.
[12] Z. Lü, D. Jiang, J. Zhang, Q. Lin, Processing and properties of ZrB_2–SiC composites obtained by aqueous tape casting and hot pressing, Ceram. Int. 37 (2011) 293–301.
[13] B. Li, J. Deng, Y. Li, Oxidation behavior and mechanical properties degradation of hot-pressed $Al_2O_3/ZrB_2/ZrO_2$ ceramic composites, Int. J. Refract. Met. Hard. Mater. 27 (2009) 747–753.
[14] B. Li, J. Deng, Z. Wu, Effect of cutting atmosphere on dry machining performance with $Al_2O_3/ZrB_2/ZrO_2$ ceramic tool, Int. J. Adv. Manuf. Technol. 49 (2010) 459–467.
[15] S. Postrach, J. Pötschke, Pressureless sintering of Al_2O_3 containing up to 20 vol.% zirconium diboride (ZrB_2), J. Eur. Ceram. Soc. 20 (2000) 1459–1468.
[16] X. Zhang, W. Li, C. Hong, W. Han, J. Han, A novel development of ZrB_2/ZrO_2 functionally graded ceramics for ultrahigh-temperature application, Scripta Mater. 59 (2008) 1214–1217.
[17] C. Hong, X. Zhang, W. Li, J. Han, S. Meng, A novel functionally graded material in the ZrB_2–SiC and ZrO_2 system by spark plasma sintering, Mater. Sci. Eng. A 498 (2008) 437–441.
[18] B. Basu, J. Vleugels, O. Biest, Development of ZrO_2–ZrB_2 composites, J. Alloys Compd. 334 (2002) 200–204.
[19] T. Zhu, W. Li, X. Zhang, P. Hu, C. Hong, L. Weng, Damage tolerance and R-curve behavior of ZrB_2–ZrO_2 composites, Mater. Sci. Eng. A 516 (2009) 297–301.
[20] N. Setoudeh, N.J. Welham, Formation of zirconium diboride by room temperature mechanochemical reaction between ZrO_2, B_2O_3 and Mg, J. Alloys Compd. 420 (2006) 225–228.
[21] D.D. Radev, D. Klissurski, Mechanochemical synthesis and SHS of diborides of titanium and zirconium, J. Mater. Synth. Process. 9 (2001) 131–136.
[22] D. Ağaoğulları, H. Gökçe, İ. Duman, M.L. Öveçoğlu, Characterization investigations of ZrB_2/ZrC ceramic powders synthesized by mechanical alloying of elemental Zr, B and C blends, J. Eur. Ceram. Soc. (2011), in press.
[23] H.Y. Ryu, H.H. Nersisyan, J.H. Lee, Preparation of zirconium-based ceramic and composite fine-grained powders, Int. J. Refract. Met. H. 30 (2012) 133–138.
[24] A.A. Kern, A.A. Coelho, Bruker-AXS TOPAS V.3.0, 2006 www.brukeraxs.com.
[25] V.L. Solozhenko, O.O. Kurakevych, A.R. Oganov, On the hardness of a new boron phase, orthorhombic γ-B_{28}, J. Super Hard Mater. 30 (2008) 428–429.
[26] V.A. Mukhanov, O.O. Kurakevych, V.L. Solozhenko, On the hardness of boron (III) oxide, J. Super Hard Mater. 30 (2008) 71–72.
[27] E.C. Subbarao, H.S. Maiti, K.K. Srivastava, Martensitic transformation in zirconia, Phys. Status Solidi A 21 (1974) 9–40.